



# Catalytic decomposition and kinetic study of mixed plastic waste

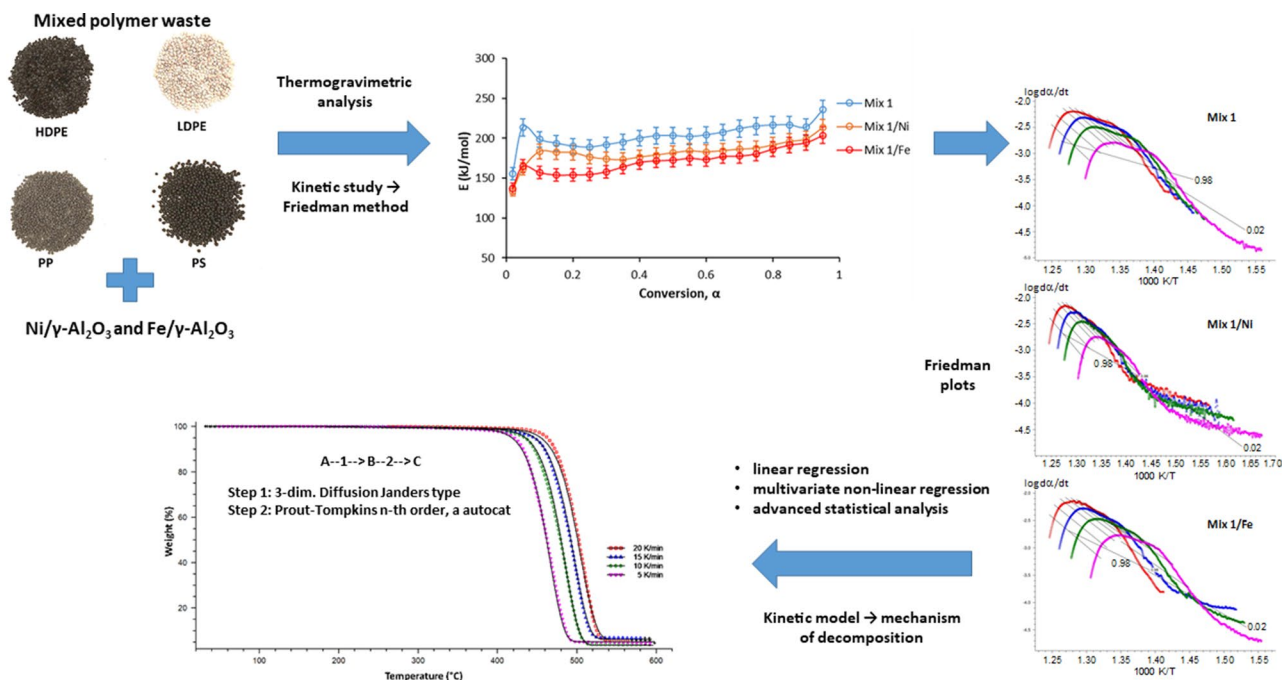
Irma Kremer<sup>1</sup> · Tihomir Tomić<sup>1</sup> · Zvonimir Katančić<sup>2</sup> · Zlata Hrnjak-Murgić<sup>2</sup> · Matko Erceg<sup>3</sup> · Daniel R. Schneider<sup>1</sup>

Received: 22 January 2020 / Accepted: 23 August 2020 / Published online: 21 September 2020  
© Springer-Verlag GmbH Germany, part of Springer Nature 2020

## Abstract

Pyrolysis is a promising technology for the valorisation of plastic waste by converting it into valuable products, such as fuels and chemicals. This study aims to assess the thermogravimetric behaviour and kinetic parameters of the real-world plastic waste mixture with added nickel- and iron-based catalysts on gamma-aluminium oxide as support. Thermogravimetric measurements were carried out in a nitrogen atmosphere over a set of heating rates (5, 10, 15 and 20 °C/min) within a temperature range 40–600 °C. Kinetic analysis was performed through a combined approach by using the model-free isoconversional Friedman method and regression methods (linear and multivariate nonlinear). The kinetic analysis results showed a complex decomposition mechanism of the real-world plastic waste mixture. The average apparent activation energy for the real-world plastic waste mixture (22% high-density polyethylene, 31% low-density polyethylene, 35% polypropylene, 12% polystyrene) was 205 kJ/mol. The initial value decreased by 15.6% with the addition of iron-based gamma-aluminium oxide catalyst and only 9.8% with nickel-based gamma-aluminium oxide catalyst.

## Graphic abstract



**Keywords** Plastic waste · Pyrolysis · Dynamic thermogravimetric analysis · Kinetic study · Catalyst

✉ Irma Kremer  
irma.kremer@fsb.hr

Extended author information available on the last page of the article

## Abbreviations

HDPE High-density polyethylene  
LDPE Low-density polyethylene

|     |                               |
|-----|-------------------------------|
| PP  | Polypropylene                 |
| PS  | Polystyrene                   |
| PVC | Polyvinyl chloride            |
| PET | Polyethylene terephthalate    |
| TGA | Thermogravimetric analysis    |
| DTG | Differential thermogravimetry |

### List of symbols

|                  |  |
|------------------|--|
| $\alpha$         | Degree of conversion (dimensionless)   |
| $\beta$          | Linear heating rate ( $^{\circ}\text{C}/\text{min}$ )                          |
| $A$              | Frequency or pre-exponential factor ( $\text{min}^{-1}$ )                      |
| $E$              | Energy of activation ( $\text{J}/\text{mol}$ )                                 |
| $f(\alpha)$      | Mechanism of reaction; kinetic model (dimensionless)                           |
| $m_0$            | Initial mass of the sample (wt%)   |
| $m_f$            | Residual mass of the sample; final mass of the residue (wt%)                   |
| $R$              | General gas constant ( $\text{J}/\text{mol K}$ )                               |
| $r_{\text{max}}$ | Maximum peak rate ( $\%/ \text{min}$ )   |
| $T$              | Absolute temperature ( $\text{K}$ )  |
| $T_{\text{max}}$ | Temperature of maximum decomposition rate and peak rate ( $^{\circ}\text{C}$ ) |

## Introduction

In 2018, in Europe, 29 Mt of post-consumer plastic waste was collected, of which 32% was recycled, 43% was energy recovered mostly by incineration and 25% was landfilled (PlasticsEurope 2019).

In previous research, the emphasis has been put on environmental sustainability in waste management which is also accentuated through the EU legislature (Tomić and Schneider 2018). There are two approaches to solving waste management problem; material and energy recovery. These approaches strive to fulfil different needs within the circular economy concept and complement each other. Although material recovery is more sustainable, energy recovery has fewer requirements for the uniformity of input material. These two approaches can be connected through pyrolysis, which can be categorised as chemical recycling. Pyrolysis is an effective technology for recovery of polymer wastes which are challenging to depolymerise or mechanically recycle, e.g. mixed plastic, polyurethane or fibre-reinforced composites (Ragaert et al. 2017). Instead of disposal, plastic solid waste can be converted into valuable products, such as fuels, chemicals and energy by pyrolysis process. Main products of the pyrolysis process are oil, gas and char (Anuar Sharuddin et al. 2016).

Different waste treatment technologies have been compared in previous research. Benavides et al. (2017) identified pyrolysis as technology that gives more environmental benefits, e.g. reduction in fossil fuel consumption and greenhouse

gas emissions. Khoo (2019) concluded that the integration of pyrolysis in the waste management system could increase environmental sustainability. The benefits of pyrolysis recovery of different types of waste have been identified. The analysis of organic waste pyrolysis showed a reduction in carbon dioxide emissions (El Hanandeh 2013). Antelava et al. (2019) concluded that in the treatment of municipal waste, pyrolysis showed better environmental results than incineration. Zaman (2010) showed that pyrolysis provides various assets in managing of solid plastic waste generated by municipalities.

A packaging industry makes up for almost 40% of European plastic converter demand. Most widely used polymers in the packaging industry are high-density and low-density polyethylene (HDPE and LDPE), polypropylene (PP), polystyrene (PS), polyvinyl chloride (PVC) and poly (ethylene terephthalate) (PET) (PlasticsEurope 2019). Among these polymers, PVC and PET are not preferable feedstock for pyrolysis. During pyrolysis of PVC, hydrochloric acid (HCl) is formed, which can lead to corrosion of the process equipment. The dechlorination process is needed, which leads to additional costs. One of the products of PET pyrolysis is benzoic acid, which is unfavourable as it can cause clogging of piping and heat exchanger (Anuar Sharuddin et al. 2016). Roozbehani et al. (2017) investigated catalytic pyrolysis, including all aforementioned polymers but avoided these issues through the use of low ratios of PVC (3%) and PET (2%) in the mixture. A recent study analysed the pyrolysis of manually sorted post-consumer plastic waste containing HDPE, PP, PS and PET collected from the municipal waste site (Singh et al. 2019a, b). The research confirmed the formation of benzoic acid, which degraded the quality of the product. In another one, the same materials were used with LDPE as an additional component. The ratio of PET was limited to only 5%, which still yielded good quality of the product (Singh et al. 2019a, b). Numerous studies were conducted using PE and PP (Sakaki et al. 2014) and PS (Imani Moqadam et al. 2015). These studies focused only on the products of pyrolysis process but did not investigate the kinetic mechanisms.

The study of pyrolysis kinetics is essential for the development of industrial-scale pyrolysis reactors. In a few studies, thermogravimetric analysis was used for determination of kinetic parameters of mixed plastics thermal decomposition. One research (Das and Tiwari 2017) dealt with neat polymers (LDPE, HDPE and PP) and made a comparative study of various isoconversional model-free methods to obtain kinetic parameters. Another similar study (Diaz Silvarrey and Phan 2016) investigated neat polymers (LDPE, HDPE, PP and PS) also with isoconversional model-free methods. The step forward was made in the kinetic study of a three-component mixture (PE, PP and PS) using isoconversional model-free method (Straka

et al. 2017). It is essential to mention that the kinetics of the pyrolysis process can be changed with the addition of catalysts.

The catalytic process requires lower temperatures, and obtained products achieve high quality in the range of motor engine fuels. Catalysts generally lower the activation energy of plastics conversion to hydrocarbons which leads to the decreased energy consumption of a conversion process. Activation energy is the minimal amount of energy needed to start a chemical reaction (Al-Salem et al. 2017). The most widely used catalysts are zeolites like Zeolite Socony Mobil-5 (ZSM-5 and HZSM-5), Fluid Catalytic Cracking (FCC), natural zeolite (NZ) and other catalysts such as aluminium oxide ( $\text{Al}_2\text{O}_3$ ) and metal oxides mixture called Red Mud (Miandad et al. 2016).

Pyrolysis processes of plastics or co-pyrolysis of plastics with biomass were also conducted using catalysts. Zhang et al. (2014) used a gamma-aluminium oxide catalyst ( $\gamma\text{-Al}_2\text{O}_3$ ) to improve hydrocarbon yield in the process of catalytic co-pyrolysis of biomass and PE, PP and PS. Another co-pyrolysis process of biomass and plastic waste was catalysed with HZSM-5/sodium carbonate/ $\gamma\text{-Al}_2\text{O}_3$  catalyst to increase yields of valuable aromatic chemicals (Ghorbannezhad et al. 2020). In some other experiments, catalyst  $\gamma\text{-Al}_2\text{O}_3$  was used as support for nickel (Ni)-based catalysts (Yao et al. 2018). Ni-based catalysts are suitable for thermal conversion of hydrocarbons because of their efficient catalytic activity and lower prices. Miskolczi et al. (2017) used nickel/molybdenum- $\text{Al}_2\text{O}_3$  catalyst and zeolites to obtain fuel and other gaseous products through pyrolysis of plastic waste on lower temperatures (under 600 °C). Waste plastics used in the process were end-of-life vehicle plastics consisting mainly of PE and PP. Besides Ni-based, iron (Fe)-based (Acomb et al. 2016) catalysts are also used for hydrogen production at higher temperatures (over 600 °C). Iron/caesium- $\text{Al}_2\text{O}_3$  catalyst can be used to convert plastic waste into chemicals and fuel additives (Wang et al. 2020).

The main hypothesis of this research is that the average apparent activation energy of real-world plastic waste mixture can be lowered with the addition of Ni- or Fe-based catalysts on  $\gamma\text{-Al}_2\text{O}_3$  as support. The decrease in activation energy means that less energy is required to carry out the pyrolysis process. The hypothesis can be proven by conducting an isoconversional model-free method of kinetic analysis. The kinetics of the real-world plastic waste mixture using the aforementioned catalysts has not been investigated yet, which sets the goal of this study. The linear and multivariate nonlinear regression method in combination with the isoconversional kinetic method yields the results of the reaction mechanism useful for the process scale-up.

## Materials and methods

The materials used for this experiment were obtained from a plastics recycling company Pos-Plast (Vrbovec, Croatia) which collects, separates and recycles post-consumer plastics. Recycled polymers HDPE, LDPE, PP and PS were received in the form of granulate. The mixture of plastics Mix 1 was prepared according to ratios of waste post-consumer plastics found in Europe. Data were collected and analysed from the Plastic-The Facts report (EU28 + Norway/Switzerland) (PlasticsEurope 2019). A variation (Mix 2) on the original real-world plastic waste mixture (Mix 1) was made, and both are presented in Table 1. Samples Mix 1 and Mix 2 were selected to investigate the reaction mechanisms of thermal decomposition process in the presence or absence of PS. Polymer granulates were weighed, extruded in Rondol Bench-top 21 mm Twin Screw extruder (Rondol Technology, Ltd., Great Britain) and finally pelletised into small pieces.

Monometallic Ni- or Fe-based catalysts were prepared using an impregnation method. The crystalline form of alumina  $\gamma\text{-Al}_2\text{O}_3$  mesoporous catalyst and metal nitrates (both purchased from Sigma-Aldrich, Missouri, US) were used as the support material. Monometallic Ni/ $\gamma\text{-Al}_2\text{O}_3$  catalyst was prepared by dissolving 5.5 g of nickel(II) nitrate hexahydrate,  $\text{Ni}(\text{NO}_3)_2 \cdot 6\text{H}_2\text{O}$ , in ethanol and addition of 10 g of  $\gamma\text{-Al}_2\text{O}_3$ , so that the initial metal loading was 10 wt%. That mixture was stirred for 4 h using a magnetic stirrer and afterwards left to dry overnight at 50 °C to remove the remaining ethanol. The solid was calcined for 3 h at 800 °C under an air atmosphere. The other catalyst, Fe/ $\gamma\text{-Al}_2\text{O}_3$ , was synthesised analogously using iron(III) nitrate nonahydrate,  $\text{Fe}(\text{NO}_3)_3 \cdot 9\text{H}_2\text{O}$ . Both catalysts were then crushed into smaller pieces.

The methods; Fourier Transform Infrared Spectroscopy, X-ray Powder Diffraction and Scanning Electron Microscopy, are used to characterise prepared catalysts.

**Table 1** Mixtures of polymers used in the experiment

| Sample | HDPE | LDPE | PP  | PS  |
|--------|------|------|-----|-----|
|        | wt%  |      |     |     |
| HDPE   | 100  | –    | –   | –   |
| LDPE   | –    | 100  | –   | –   |
| PP     | –    | –    | 100 | –   |
| PS     | –    | –    | –   | 100 |
| Mix 1  | 22   | 31   | 35  | 12  |
| Mix 2  | 28   | 37   | 35  | 0   |

## Fourier transform infrared spectroscopy

FTIR spectra were obtained using transmission technique with samples mixed with KBr and pressed to pellet, using a Spectrum One FTIR spectrometer (Perkin Elmer, Inc., Massachusetts, United States) in the wavenumber range from 4000 to 450  $\text{cm}^{-1}$  and resolution of 4  $\text{cm}^{-1}$ .

## X-ray powder diffraction

The crystal phases in prepared samples were identified by X-ray diffraction using the XRD 6000 (Shimadzu, Japan) with  $\text{CuK}\alpha$  radiation of 40 kV and current of 30 mA, in the  $2\theta$  range  $10^\circ$ – $70^\circ$  and with a step of  $0.02^\circ$  and a scan speed of  $2^\circ/\text{min}$ .

## Scanning electron microscopy

Morphology of catalysts was analysed using SEM JSM 7000F (JEOL, California, United States). An accelerating voltage of 10 kV was used to collect the micrographs.

## Dynamic thermogravimetry

The experiments were conducted in Q500 thermogravimetric analyser (TA Instruments, Delaware, US) to measure the change in mass of sample with temperature during pyrolysis reaction. The studies were carried out in nitrogen flow (60  $\text{cm}^3/\text{min}$ ) over a set of heating rates (5, 10, 15 and 20  $^\circ\text{C}/\text{min}$ ) within a temperature range 40–600  $^\circ\text{C}$ . First, granulates of each polymer type were analysed, then mixtures, and in the end mixtures with catalysts. Mass of mixture pellets was 10–12 mg.

## Kinetics of the thermal decomposition of polymer materials

The kinetic study needs to be conducted to describe the mechanism of the thermal decomposition (pyrolysis). Thermal decomposition of polymers and polymer materials can be classified into solid-state reactions (Erceg et al. 2018). The experimental data for kinetic analysis in this work are obtained by dynamic thermogravimetry. The progress of the thermal decomposition can be expressed by the conversion,  $\alpha$ , shown in Eq. (1):

$$\alpha = \frac{m_0 - m}{m_0 - m_f} \quad (1)$$

where  $m_0$  is the initial,  $m$  is actual, and  $m_f$  is a residual mass of the sample. The value of  $\alpha$  represents the progress of the overall conversion of reactants to products; in this case, the progress of the thermal decomposition process. It is possible to carry out a kinetic study using experimental  $\alpha$ – $T$  (temperature) data obtained at minimum 3–5 heating rates, as advised by the ICTAC Kinetics Committee (Vyazovkin et al. 2011).

Kinetics of the single process reactions in solid-state can be described by Eq. (2) (Vyazovkin et al. 2011):

$$\frac{d\alpha}{dt} \cong \beta \frac{d\alpha}{dT} = A \cdot \exp\left(-\frac{E}{RT}\right) \cdot f(\alpha) \quad (2)$$

where  $t$  is time (min),  $\beta$  is the linear heating rate ( $^\circ\text{C}/\text{min}$ ),  $T$  is the absolute temperature (K), and  $R$  is the general gas constant ( $\text{J}/\text{molK}$ ). Kinetic parameters are;  $A$ , frequency or pre-exponential factor ( $1/\text{min}$ ),  $E$ , the activation energy ( $\text{J}/\text{mol}$ ) and  $f(\alpha)$ , the mechanism of reaction (kinetic model). The calculated kinetic parameters can be defined as apparent to emphasise the fact that they can differ from the intrinsic parameters of a specific step (Vyazovkin et al. 2011).

It is suggested by the ICTAC Kinetics Committee (Vyazovkin et al. 2011) to study the complexity of the process before conducting any kinetic analysis. The complexity of the process is investigated by determination of the dependence of  $E$  on  $\alpha$  using isoconversional model-free methods. Isoconversional methods are known for being the most reliable methods for the calculation of  $E$  (Vyazovkin S and Lesnikovich 1990, Vyazovkin and Sbirrazzuoli 2006, Vyazovkin et al. 2011). If  $E$  is not dependent on  $\alpha$ , then the studied process is simple (overall single stage). It can be described by a single reaction model and a single pair of Arrhenius parameters. The linear model-fitting method can be used for the determination of  $A$  and  $f(\alpha)$ . If the process is complex, meaning that  $E$  greatly varies with  $\alpha$ , the reaction model and Arrhenius parameters must be computed for each particular reaction step. This can be accomplished using model-fitting methods (nonlinear regression) or by specifically developed software like Netzsch Thermokinetics (Rotaru et al. 2008) or Thermal and Kinetic Software (Rotaru and Goşa 2009). In this research, values of  $E$  for all samples have been calculated using the isoconversional Friedman (FR) method (Friedman 1964) incorporated into Netzsch Thermokinetics 3.0 software (Netzsch Group, Germany). It is a model-free method which means that  $E$  and  $E$ – $\alpha$  dependence can be determined without knowledge about the kinetic model. Friedman method (Friedman 1964) is a linear differential method expressed by Eq. (3):

$$\ln\left[\beta \frac{d\alpha}{dT}\right] = \ln A + \ln f(\alpha) - \frac{E}{RT} \quad (3)$$



The plot  $\ln [\beta(d\alpha/dT)]$  versus  $1/T$  obtained from experimental  $\alpha - T$  data should be straight lines from whose slopes it is possible to calculate  $E$  for each selected  $\alpha = \text{const}$ .

In this work, kinetic study was carried out using Netzsch Thermokinetics 3.0 software. Linear regression was used for simple, single-stage processes, while multivariate nonlinear regression was used for complex, multi-stage processes together with advanced statistical analysis. Both methods focus on fitting a great number of reaction models (Table 2) to experimental thermogravimetric data. This table contains usual models for homogeneous and solid-state reactions. The well-known reaction types' list (Vyazovkin et al. 2011) is expanded with the combined autocatalytic types C1 and Cn (Opfermann 2000). When the model gives the smallest difference between the experimental and computed values, it is considered as the most suitable one. This is evaluated using statistical methods, least squares method and  $F$ -test. It should be taken into account that a statistically most suitable model does not always interpret the mechanism of the investigated process in the best way. It is advisable to compare the  $E$  values with the ones calculated with the isoconversional methods. The model can be considered as a true kinetic model of the investigated process if the  $E$  value corresponds to the statistically most suitable model, and it is in a good correlation with  $E$  values obtained by the isoconversional methods (Stipanelov Vrandečić et al. 2010).

## Results and discussion

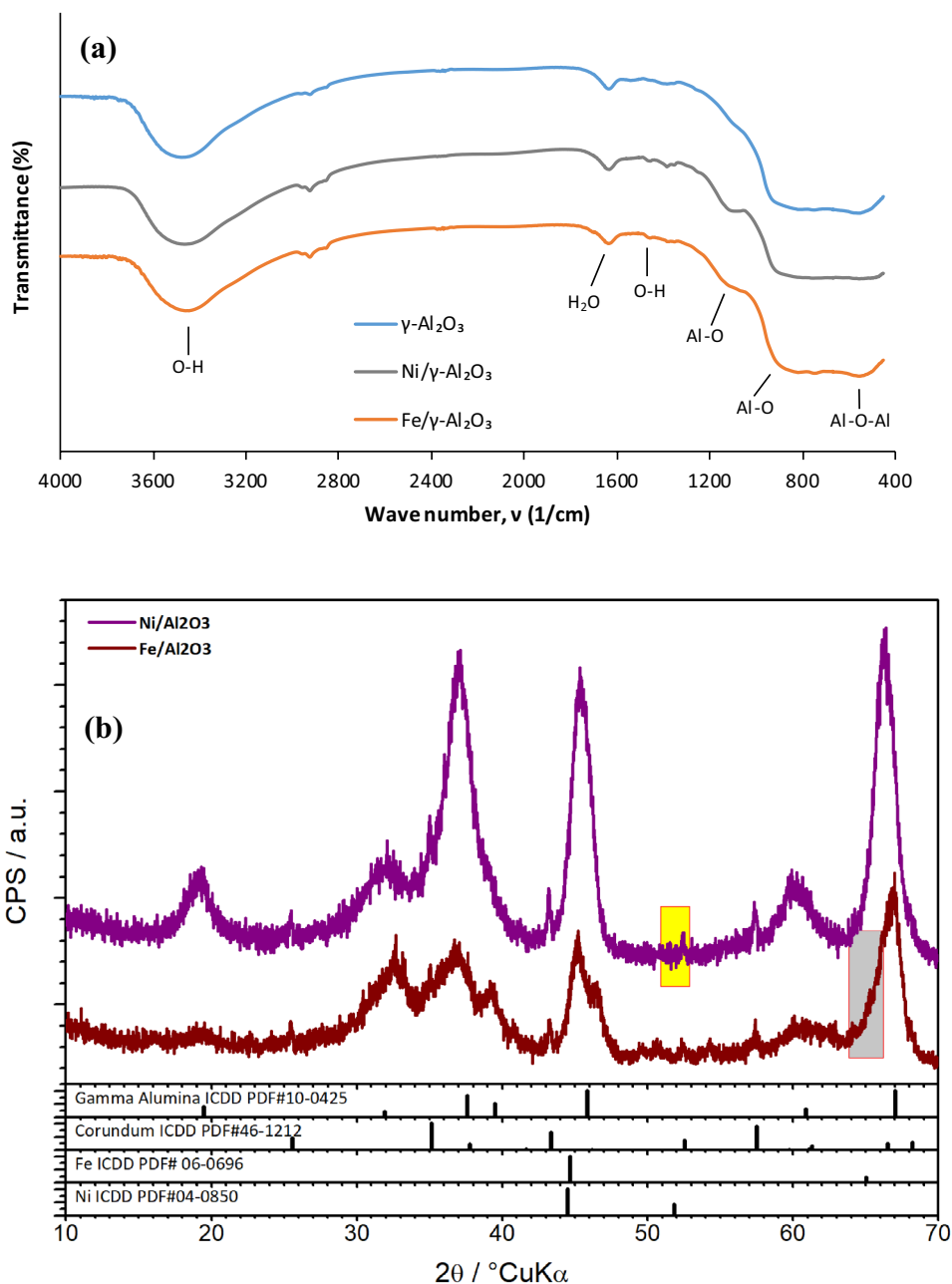
Obtained FTIR spectra of  $\gamma\text{-Al}_2\text{O}_3$ , Ni/ $\gamma\text{-Al}_2\text{O}_3$  and Fe/ $\gamma\text{-Al}_2\text{O}_3$  catalysts are presented in Fig. 1a. Characteristic absorption peaks of neat  $\gamma\text{-Al}_2\text{O}_3$  have been identified as follows (Riad 2007): the broad band at 3200–3700  $\text{cm}^{-1}$  represents the stretching vibration of -OH that is bonded to  $\text{Al}^{3+}$ , and the peak at 1635  $\text{cm}^{-1}$  can be assigned to physisorbed water. The following peaks at 1385  $\text{cm}^{-1}$  and 1355  $\text{cm}^{-1}$  can be observed due to water deformation vibrations (-OH). At 1100  $\text{cm}^{-1}$ , a band characteristic for  $\gamma$ -alumina appears due to Al-O vibration mode. The  $\gamma$ -form is confirmed by the typical valley between 1000  $\text{cm}^{-1}$  and 435  $\text{cm}^{-1}$ . The peak at 820  $\text{cm}^{-1}$  corresponds to the bending vibrations of Al-O bond, while the peak at 550  $\text{cm}^{-1}$  can be assigned to Al-O-Al bond in the gamma phase of alumina. No additional absorption peaks can be observed when comparing neat  $\gamma\text{-Al}_2\text{O}_3$  spectra to the ones of Ni/ $\gamma\text{-Al}_2\text{O}_3$  and Fe/ $\gamma\text{-Al}_2\text{O}_3$ . It is possible that metals (Ni and Fe) are not detectable by FTIR spectroscopy because of the low metal loading (10 wt%) on  $\gamma\text{-Al}_2\text{O}_3$ .

The high-angle XRD patterns of Ni/ $\gamma\text{-Al}_2\text{O}_3$  and Fe/ $\gamma\text{-Al}_2\text{O}_3$  catalysts are shown in Fig. 1b. The results of the XRD patterns were compared to the laboratory database for  $\gamma$ -alumina, corundum (a crystalline form of  $\text{Al}_2\text{O}_3$ ), Ni and Fe. From Fig. 1b, it can be seen that diffraction peaks of Ni and Fe are mostly covered by strong  $\gamma$ -alumina and corundum peaks. The main peaks of Fe and Ni are at 44.5°, which is very close to the dominant peak of  $\gamma$ -alumina at 46°. The second peak for Fe is found at 65° (grey square), which is again close to  $\gamma$ -alumina at 67°.

**Table 2** Reaction model types and corresponding reaction equations  $de/dt = -A \exp(E/RT)f(e, p)$

| Code     | $f(e, p)$                   | Reaction type  |
|----------|-----------------------------|--|
| F1       | $e$                         | First-order reaction   |
| F2       | $e^2$                       | Second-order reaction  |
| F $n$    | $e^n$                       | $n$ th-Order reaction  |
| R2       | $2e^{1/2}$                  | Two-dimensional phase boundary reaction  |
| R3       | $3e^{2/3}$                  | Three-dimensional phase boundary reaction  |
| D1       | $0.5/(1 - e)$               | One-dimensional diffusion  |
| D2       | $-1/\ln(e)$                 | Two-dimensional diffusion  |
| D3       | $1.5e^{1/3}/(e^{-1/3} - 1)$ | Three-dimensional diffusion (Jander' type)   |
| D4       | $1.5/(e^{-1/3} - 1)$        | Three-dimensional diffusion (Ginstling-Brounstein type)  |
| B1       | $ep$                        | Simple Prout-Tompkins equation   |
| B $na$   | $e^n p^a$                   | Expanded Prout-Tompkins equation ( $na$ )  |
| C1-X     | $e(1 + KcatX)$              | First-order reaction with autocatalysis through the reactants, X<br>X = a product in the complex model, frequently $X = p$ |
| C $n$ -X | $e^n(1 + KcatX)$            | $n$ th-Order reaction with autocatalysis through the reactants, X  |
| A2       | $2e(-\ln(e))^{1/2}$         | Two-dimensional nucleation   |
| A3       | $3e(-\ln(e))^{2/3}$         | Three-dimensional nucleation   |
| A $n$    | $ne(-\ln(e))^{(n-1)/n}$     | $n$ -Dimensional nucleation/nucleus growth according to Avrami-Erofeev   |

**Fig. 1** **a** FTIR spectra and **b** XRD patterns of Ni/ $\gamma$ -Al<sub>2</sub>O<sub>3</sub> and Fe/ $\gamma$ -Al<sub>2</sub>O<sub>3</sub> catalysts



Only a small prominence in XRD spectra of Ni/Al<sub>2</sub>O<sub>3</sub> (yellow square) at 52° suggests the possible presence of Ni. It can be concluded that it was not possible to confirm the presence of metals on the support with the great certainty using XRD analysis.

In Fig. 2, SEM images and EDS graphs of Ni/ $\gamma$ -Al<sub>2</sub>O<sub>3</sub> and Fe/ $\gamma$ -Al<sub>2</sub>O<sub>3</sub> catalysts are shown, and the results of EDS elemental analysis are listed in Table 3. A similar morphology is observed in both samples; smaller agglomerated particles of metals can be seen on the surface of  $\gamma$ -Al<sub>2</sub>O<sub>3</sub> (Fig. 2). EDS elemental analysis confirms the presence of metals and the metal loading of approximately 10 wt% on  $\gamma$ -Al<sub>2</sub>O<sub>3</sub> (Table 2).

## Thermogravimetric analysis

In “Appendix”, Fig. 9 shows a mass loss (thermogravimetric, TG curves) and derivative mass loss (derivative thermogravimetric, DTG curves) at four heating rates for neat polymers. The values of peak decomposition temperature, peak height and residue mass for all neat polymers can be found in an “Appendix” in Table 5. It is visible from DTG plots that the peak decomposition temperature and peak height are increasing with the increase of the heating rate for all neat polymers (Fig. 9). At higher heating rates polymers are decomposing over a wider temperature range (broader peak) and demand higher pyrolysis temperature to achieve

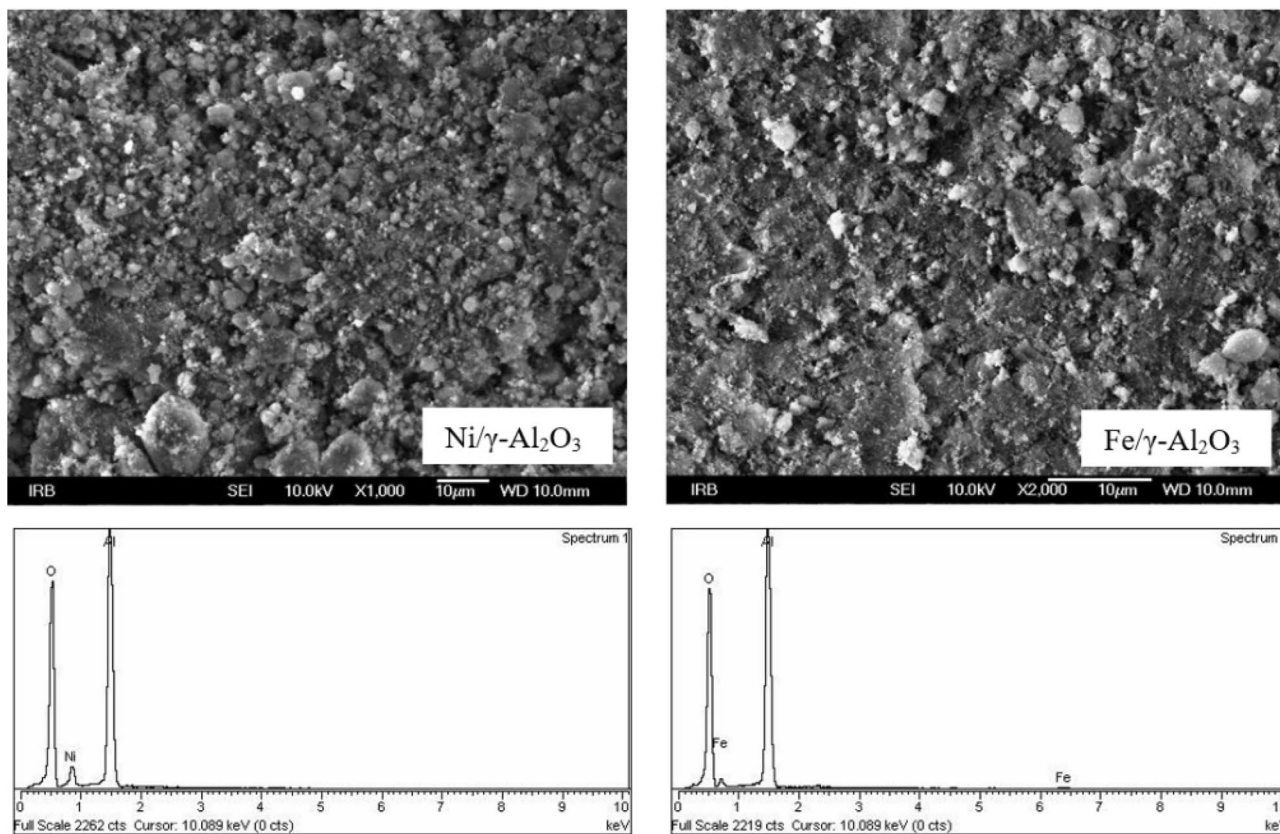


**Fig. 2** SEM images and EDS graphs of Ni/ $\gamma$ -Al<sub>2</sub>O<sub>3</sub> and Fe/ $\gamma$ -Al<sub>2</sub>O<sub>3</sub> catalysts

**Table 3** EDS elemental analysis of Ni/ $\gamma$ -Al<sub>2</sub>O<sub>3</sub> and Fe/ $\gamma$ -Al<sub>2</sub>O<sub>3</sub> catalysts

| Sample                                       | Element | wt%   | Atomic (%) |
|--|---------|-------|------------|
| Ni/ $\gamma$ -Al <sub>2</sub> O <sub>3</sub> | O K     | 46.96 | 62.52      |
|  | Al K    | 42.75 | 33.74      |
|  | Ni K    | 10.29 | 3.73       |
| Fe/ $\gamma$ -Al <sub>2</sub> O <sub>3</sub> | O K     | 46.58 | 61.89      |
|  | Al K    | 43.67 | 34.4       |
|  | Fe K    | 9.75  | 3.71       |
| Totals                                       |         |       | 100        |

the same conversion. Examination of data implies that all investigated polymers decompose in a single-stage process with a shift to higher temperatures at higher heating rates. That is following the findings in the literature (Diaz Silveira and Phan 2016).

Figure 10 represents TG and DTG curves of HDPE, LDPE, PP and PS (neat polymers) at the heating rate of 10 °C/min. The decomposition of each polymer is a single-stage process occurring in the temperature range 350–500 °C. The thermal stability increases in the following order: PS < PP < LDPE < HDPE. The peak decomposition

temperatures are 429 °C, 458 °C, 473 °C and 477 °C, respectively. Values of residue masses are low and vary from 2.3 to 4.6 wt%.

DTG plots for Mix 1 and Mix 2 without and with catalysts are shown in Fig. 3. Additional data about decomposition (peak decomposition temperature, peak height and residue mass) can be found in an “Appendix” in Table 6. It is noticeable that the DTG curves are following the same pattern as the ones of neat polymers. Comparatively, the peak decomposition temperature and peak height are increasing as the heating rate increases. From DTG plot of Mix 1, it is visible that the thermal decomposition is occurring in two stages. The first stage of decomposition attributes to the decomposition of PS, which decomposes at lower temperatures. The second stage corresponds to HDPE, LDPE and PP and their decomposition products. These decomposition products, together with decomposition products of PS, shift the maximum decomposition rate to higher temperatures than the ones of neat polymers. The shape of the peak in the DTG plot of Mix 1 is also changing as heating rate increases. The first stage of decomposition for Mix 1 is less apparent at higher heating rates. The peak area is proportional to the change of mass ( $\alpha$ ) and the rate of reaction ( $da/dt$ ). The rate of reaction depends on kinetic triplet ( $E$ ,  $f(\alpha)$ ,  $A$ ) as stated

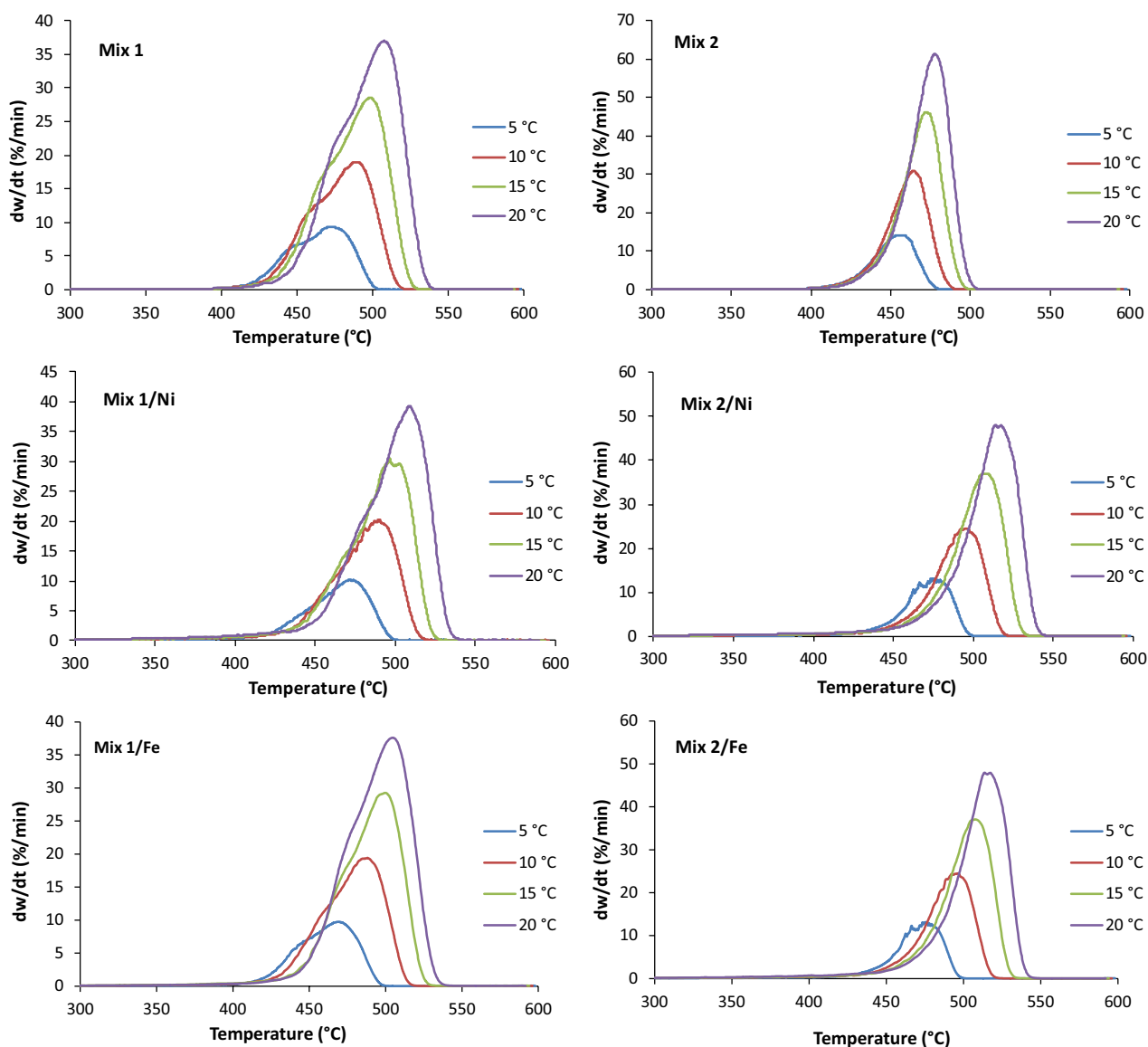


**Fig. 3** Derivative thermogravimetric plots for Mix 1, Mix 2, Mix 1/Ni, Mix 2/Ni, Mix 1/Fe and Mix 2/Fe at 5, 10, 15 and 20 °C/min

in Eq. (2). While  $E$  and  $A$  are functions of temperature,  $f(\alpha)$  is a mathematical function that describes how the mass changes (the mechanism of the reaction). If the shape of a peak changes, it means that the mass changes differently, and it indicates a different mechanism of reaction (Diaz Silvarrey and Phan 2016). From DTG plot of Mix 2, it is clear that the decomposition is happening in one stage. That is because PS was not added to that mixture. It could also be concluded that Mix 1 sample has higher thermal stability than Mix 2 since the decomposition of the main stage in Mix 1 is shifted to higher temperatures.

From DTG plots (Fig. 3) of Mix 1/Ni and Mix 2/Ni samples (mixtures with Ni/ $\gamma$ -Al<sub>2</sub>O<sub>3</sub> catalyst), it is visible that the thermal stability of both samples is very similar. It is

noticeable that the first stage of decomposition of Mix 1/Ni is less apparent in comparison with the mixture without a catalyst. That implies that the catalyst had an effect on the decomposition of PS and shifted the first-stage decomposition towards higher temperatures. The temperature of the second-stage decomposition remained almost the same as in the mixture without the catalyst. That is not the case for the one-stage decomposition of Mix 2/Ni sample. The peak decomposition temperature increased significantly (up to 36 °C for higher heating rates, Table 6) in comparison with the mixture without the catalyst. The results with Fe/ $\gamma$ -Al<sub>2</sub>O<sub>3</sub> catalyst are very similar to the ones obtained with Ni/ $\gamma$ -Al<sub>2</sub>O<sub>3</sub> catalyst, which can be confirmed by looking into the results in Fig. 3 and Table 6. The reason behind these results



could be the fact that metals Fe and Ni have similar chemical properties. Values of residue masses are higher than the ones of mixtures without catalysts. This is expected since the catalysts used are an inorganic matter which remains in the system after being exposed to high temperatures.

## Results of the kinetics of the thermal decomposition of mixed plastics

To determine the complexity and to find the most suitable kinetic scheme of the investigated process, several approaches were used (Erceg et al. 2018);

1. Closer attention was paid to the experimental TG and DTG curves and the dependence of the residual mass on the heating rate.
2. The dependence of the activation energy computed by Friedman method ( $E_{FR}$ ) on  $\alpha$  is observed.
3. The shape of Friedman plots, the slopes of experimental points and isoconversional Friedman lines at the start of the reaction ( $\alpha = 0.02\text{--}0.10$ ) were also analysed. The number of peaks and shoulders on Friedman plots indicates the number of decomposition steps. The comparison of the slopes of experimental points and isoconversional Friedman lines at the beginning of the process (Netzsch Thermokinetics Software Manual, Selb: Netzsch-Geratebau GmbH 2014).
4. The linear or nonlinear model-fitting regression method was applied for single-step and multi-step processes, respectively.

According to approach (1), the residual mass at TG curves of the all analysed samples was observed. The residual mass does not depend on the heating rate (Fig. 9). That means that their decomposition follows unbranched reaction path (Netzsch Thermokinetics Software Manual, Selb: Netzsch-Geratebau GmbH 2014). Regarding approach (2), the results of  $E_{FR}$  versus  $\alpha$  dependence for neat polymers (Fig. 4a) show that  $E_{FR}$  values are not dependent on  $\alpha$  indicating the single-step process. It is shown earlier (section Thermogravimetric analysis) that DTG curves of all neat polymers show only one peak without shoulders. That implies a single-stage process since it is recognised that each peak or shoulder represents at least one reaction step (Vyazovkin et al. 2011). These conclusions indicate simple, single-step decomposition kinetics for neat polymers. Their decomposition process can be described by a single kinetic model. The linear regression method was used for that purpose. The highest average  $E_{FR}$  values were obtained for HDPE (231 kJ/mol), then LDPE (210 kJ/mol) and PP (192 kJ/mol), and the lowest for PS (161 kJ/mol). Both HDPE and LDPE have the

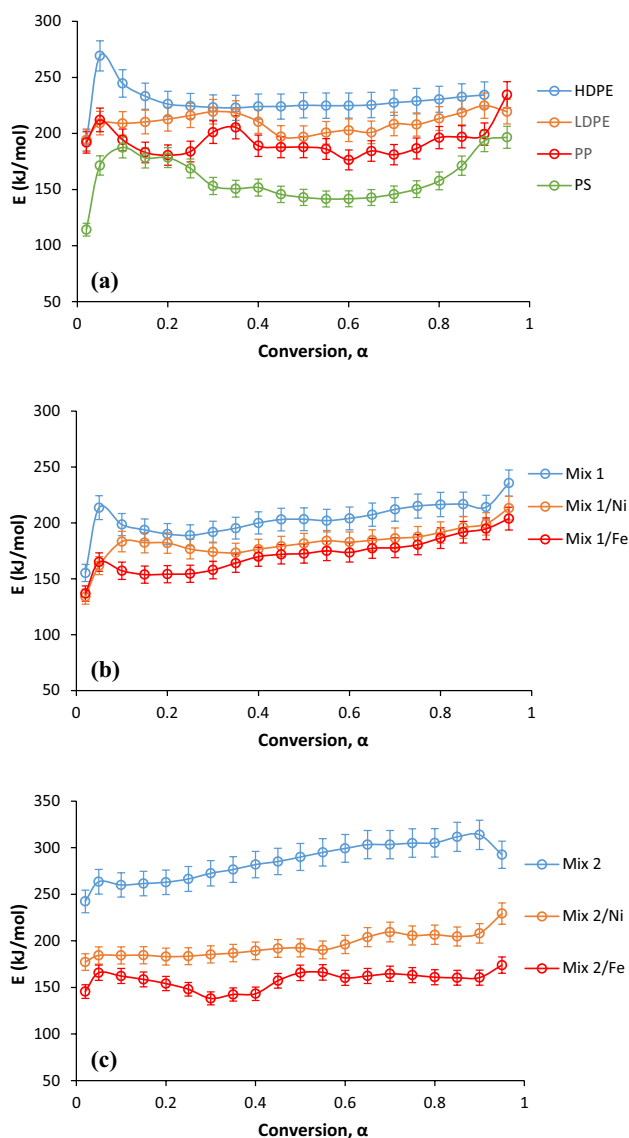


**Fig. 4** Dependence of  $E_{FR}$  on  $\alpha$  for **a** neat polymers, **b** Mix 1, Mix 1/Ni and Mix 1/Fe and **c** Mix 2, Mix 2/Ni and Mix 2/Fe

same chemical composition (saturated hydrocarbons) but a different structure. HDPE has a crystalline structure and LDPE amorphous structure; hence, there is a small difference in values of  $E_{FR}$ . The lower values of  $E_{FR}$  can be seen at the very beginning of reaction in the case of PS. That corresponds to the scission of the main chain while the rest of the reaction can be assigned to the formation of monomer styrene and polymer radicals, which further react to form oligomers (Peterson et al. 2001).

Approach (2) continues with the results of  $E_{FR}$  versus  $\alpha$  dependence for the investigated mixtures of polymers (Fig. 4b, c). The results for all Mix 1 samples (Fig. 4b) show a slight increase in  $E_{FR}$  as the conversion progresses. The value of average  $E_{FR}$  for Mix 1 sample (205 kJ/mol) which contained PS is

lower than the value of polymer HDPE and similar to values of LDPE and PP. The average  $E_{FR}$  value of Mix 1 sample decreased to 185 kJ/mol by adding the Ni/ $\gamma$ -Al<sub>2</sub>O<sub>3</sub> catalyst and 173 kJ/mol by adding the Fe/ $\gamma$ -Al<sub>2</sub>O<sub>3</sub> catalyst. In Fig. 4c, the average  $E_{FR}$  value of Mix 2 sample without catalyst shows increase similar to Mix 1 samples. Among all mixtures, values of average  $E_{FR}$  are the highest for Mix 2 (288 kJ/mol). The results for samples Mix 2/Ni and Mix 2/Fe show how  $E_{FR}$  values do not significantly vary with  $\alpha$  (Fig. 4c). The  $E_{FR}$  values of sample Mix 2 lowered to 196 kJ/mol with the addition of Ni/ $\gamma$ -Al<sub>2</sub>O<sub>3</sub> catalyst and 158 kJ/mol with Fe/ $\gamma$ -Al<sub>2</sub>O<sub>3</sub> catalyst. It may be possible that average  $E_{FR}$  value for Mix 2 is higher because of the absence of PS. According to Straka et al. (2017), PS-derived radicals can enhance the conversion of PP and PE. The thermal decomposition of HDPE/LDPE and PP with the presence of PS can be interpreted in this way; after the scission of the main chain in PS, the polymer radicals are formed as shown in Fig. 5a and b. They react with HDPE/LDPE (Fig. 5c, d) or PP (Fig. 5e, f) to produce polyethylene or PP radicals, respectively.

Produced radicals are initiating fission of following chains to generate chain radicals that propagate through numerous concurrent reactions. This action is ended through disproportional events or recombination. In the example, the

formation of alkenes with a double bond ending. Also, PP radicals with branched chain can finally form substituted alicyclic hydrocarbons.

It is shown earlier (section Thermogravimetric analysis, Fig. 3) that DTG curves of all mixtures, except Mix 2 and Mix 2/Ni, show one shoulder and one peak. That indicates a two-stage decomposition mechanism since each peak or shoulder represents at least one reaction step (Vyazovkin et al., 2011). Mix 2 and Mix 2/Ni show one peak on DTG curves (simple decomposition process).

Approach (3) analyses the experimental points at the start of the reaction ( $\alpha=0.02-0.10$ ) compared with Friedman plots obtained from experimental  $\alpha-T$  data (Eq. 3). This is shown in Figs. 6 and 7. The models mentioned in Table 2; F1, F2, Fn, R2 or R3 should be taken into account if experimental points correspond with the isoconversional ones. The diffusion models D1–D4 should be taken into consideration if the experimental points at the start show a lower slope than the isoconversional ones. The autocatalytically activated reaction type or Avrami–Erofeev reaction type is most probable if experimental points show steeper slope than the isoconversional ones (Erceg et al. 2018). In the case of HDPE, LDPE and PP, the experimental points for

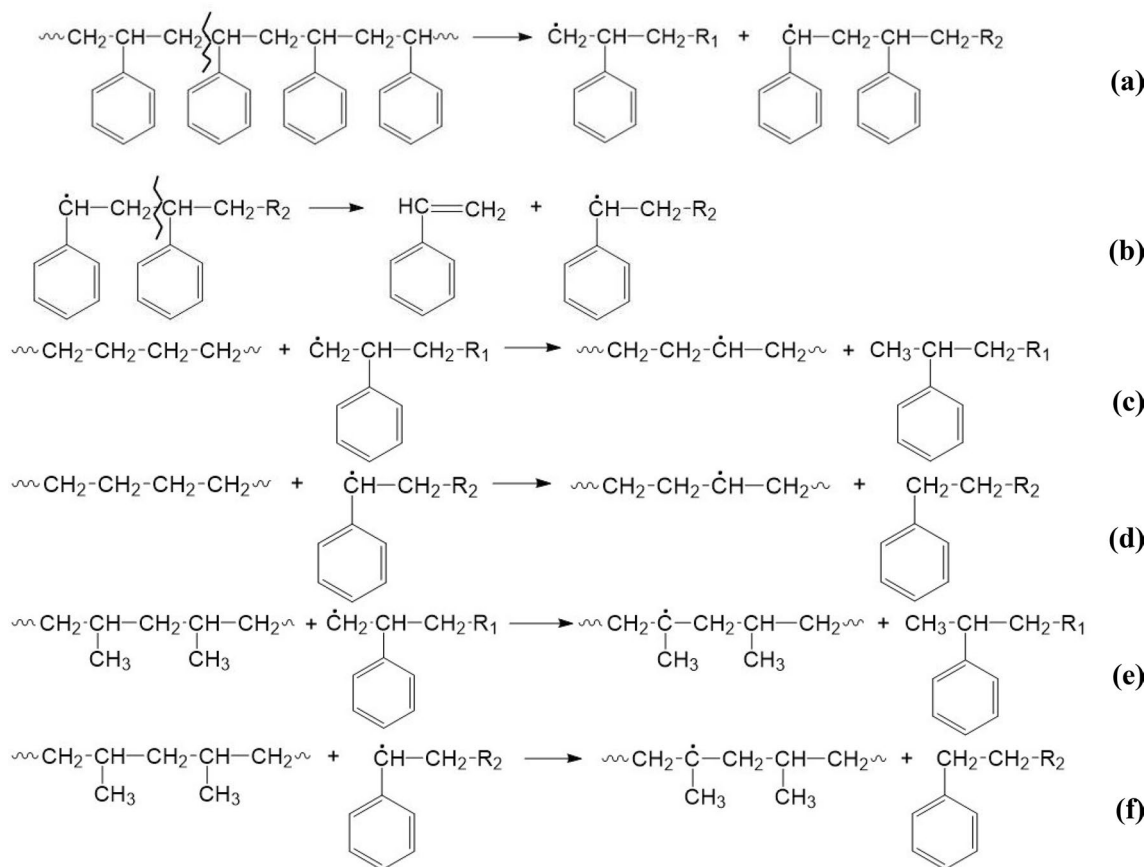
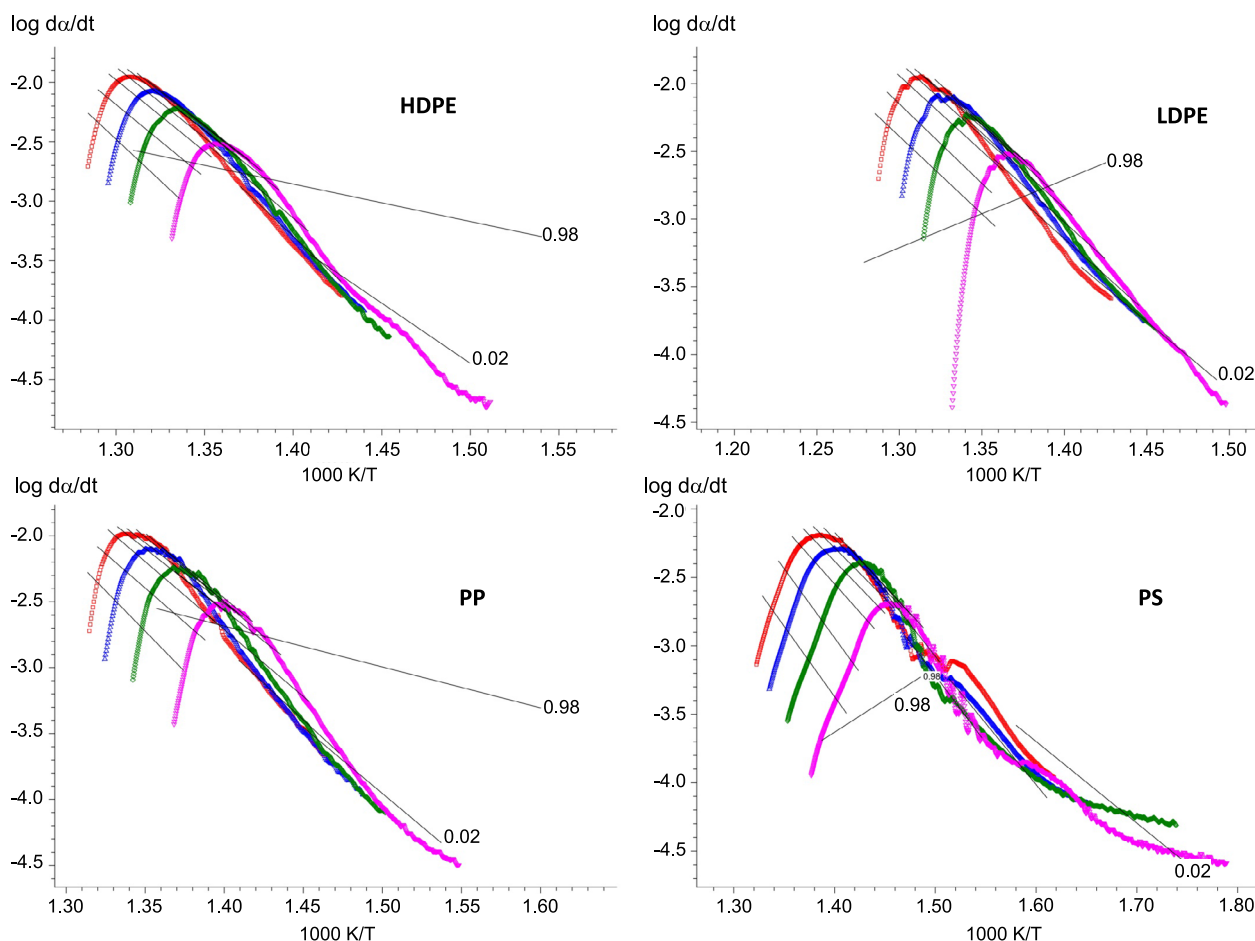


Fig. 5 Initiation reactions of thermal decomposition of a mixture of PS, polyethylene and PP



**Fig. 6** Friedman plots for the non-isothermal decomposition of neat polymers (HDPE, LDPE, PP and PS)

the non-isothermal decomposition show steeper slope than isoconversional ones. That implies an autocatalytically activated or Avrami-Erofeev reaction type (Fig. 6). Their Friedman plots are showing one peak, confirming the assumption about single-step decomposition. Regarding the results for Mix 1, the experimental points coincide with isoconversional ones pointing to F1, F2, Fn, R2 or R3 model. The experimental points of Mix 1 samples with both catalysts ( $\text{Ni}/\gamma\text{-Al}_2\text{O}_3$  and  $\text{Fe}/\gamma\text{-Al}_2\text{O}_3$ ) exhibit lower slope implying diffusion models. For the later stage of Mix 1 decomposition, the non-isothermal decomposition presumably occurs through two-step unbranched reaction path since Friedman plot shows only one additional peak (Fig. 7). The experimental points for Mix 2, as well as for Mix 2/Ni present steeper slope than the isoconversional ones indicating autocatalytically activated or Avrami-Erofeev reaction type. In the Friedman plots of these samples only one peak is visible, pointing to single-step decomposition. The diffusion reaction could be present in the case of Mix 2/Fe since the experimental points display a lower slope than isoconversional

ones. The two peaks visible in Friedman's plot for Mix 2/Fe, point to two-step non-isothermal decomposition (Fig. 7).

In approach (4), both linear and nonlinear multivariate model-fitting regression method are used for fitting a series of reaction model types listed in Table 2 to the experimental data. Linear regression is applied to the single-step processes, while nonlinear regression is applied to the complex processes. A statistical method of *F*-test is used to determine the most suitable kinetic model. The statistical analysis by any software focuses more on the quality of fit rather than to the physical meaning of calculated kinetic models. That can lead to big differences in computed activation energies. Sánchez-Jiménez et al. (2013) have shown that most kinetic models correctly fit the data, but each providing a different value for the activation energy. As it is previously concluded, isoconversional methods are the most reliable ones for the calculation of activation energy and that thus calculated values are true ones for the investigated process. The most suitable kinetic model should generate values of activation energy that are very similar to the reliable isoconversional methods.

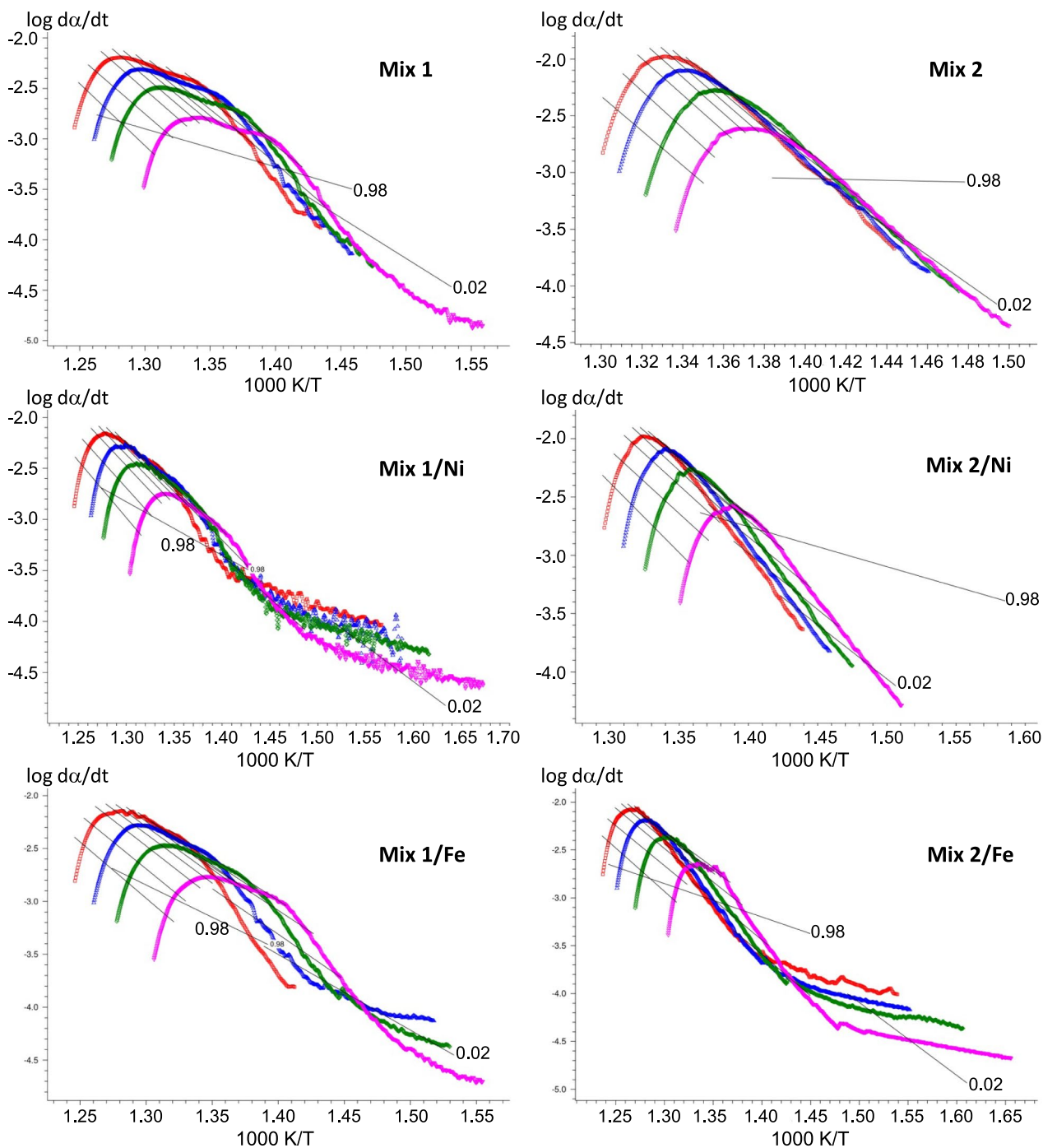


**Fig. 7** Friedman plots for the non-isothermal decomposition of Mix 1, Mix 1/Ni, Mix 1/Fe, Mix 2, Mix 2/Ni and Mix 2/Fe

Critical F-test value,  $F_{crit}$ , was calculated by Netzsch Thermokinetics 3.0 for the chosen confidence probability and the number of experimental points ( $F_{crit} = 1.04$ ). If  $F_{exp} < F_{crit}$ , then the kinetic model most probably describes the process. The kinetic analysis confirmed earlier presumption that neat polymers decompose in one decomposition step. The autocatalytically activated Cn kinetic model is found to be the most probable one since

its  $F_{exp} < F_{crit}$  (Table 4). A diffusion reaction was present at the very start of the PS decomposition reaction but in such a small conversion range that only one decomposition step (Cn kinetic model) was identified by the software. For sample Mix 1, assumption about two-step decomposition was also confirmed. Kinetic model Fn corresponds to the early stage of decomposition in the conversion range up to 10%. The next stage can be assigned to Bna model. The

**Table 4** Values of kinetic parameters ( $E$ ,  $\log A$ ) and statistical analysis ( $F$ -test) for the most suitable kinetic models and comparison with isoconversional  $E_{FR}$  values

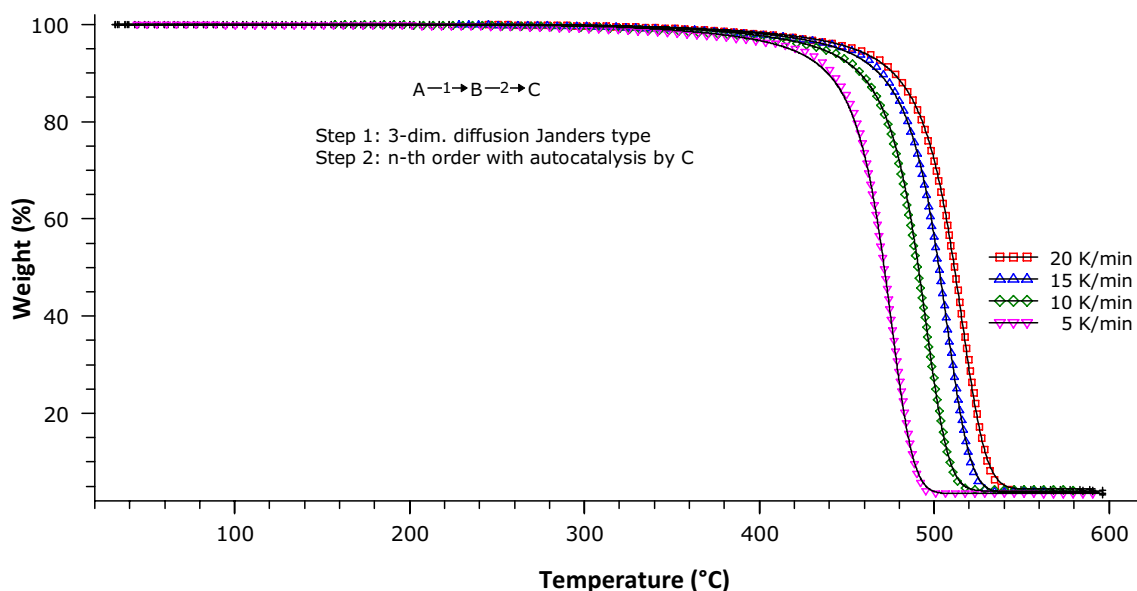
| Sample   | $f(\alpha)$   | $F_{exp}$ | $\log A$ (1/s) | $E$ (kJ/mol) | $E_{FR}$ (kJ/mol) |
|----------|---|-----------|----------------|--------------|-------------------|
| HDPE     | CnB ( $n=0.98$ ; $\log K_{cat}=0.88$ )                                  | 1.00      | 13.29          | 231          | 230               |
| LDPE     | CnB ( $n=0.96$ ; $\log K_{cat}=0.94$ )                                  | 1.00      | 11.93          | 208          | 210               |
| PP       | CnB ( $n=1.00$ ; $\log K_{cat}=1.07$ )                                  | 1.00      | 11.07          | 193          | 192               |
| PS       | CnC ( $n=1.19$ ; $\log K_{cat}=0.55$ )                                  | 1.00      | 9.50           | 161          | 161               |
| Mix 1    | Fn ( $n=1.55 \cdot 10^{-4}$ )/Bna ( $n=0.79$ ; $a=6.99 \cdot 10^{-4}$ ) | 1.00      | 10.62/11.88    | 180/204      | 205               |
| Mix 1/Ni | D3/CnC ( $n=0.89$ ; $\log K_{cat}=0.13$ )                               | 1.00      | 2.97/10.86     | 82/192       | 185               |
| Mix 1/Fe | D3/Bna ( $n=0.84$ ; $a=0.35$ )  | 1.00      | 1.14/9.30      | 56/164       | 173               |
| Mix 2    | CnB ( $n=1.11$ ; $\log K_{cat}=0.44$ )                                  | 1.00      | 17.07          | 273          | 288               |
| Mix 2/Ni | CnB ( $n=1.07$ ; $\log K_{cat}=1.12$ )                                  | 1.00      | 10.30          | 185          | 196               |
| Mix 2/Fe | D3/CnC ( $n=0.99$ ; $\log K_{cat}=0.96$ )                               | 1.00      | 6.64/8.30      | 135/162      | 158               |

diffusion model, D3, is responsible for the initial stage of decomposition of Mix 1 samples with catalysts in the conversion range up to 3.5% for Mix 1/Ni, and up to 3% for Mix 1/Fe. The kinetic models for the main stage can be attributed to Cn and Bna model, respectively. The results of kinetic analysis for Mix 2 and Mix 2/Ni samples are following the previous assumption, and their single-step decomposition can be described with autocatalytically activated Cn model. In contrast, two-step decomposition of Mix 2/Fe corresponds to D3 diffusion model in the conversion range up to 3% and Cn model in the main stage.

Table 4 presents the values of kinetic parameters ( $E$ ,  $\log A$ ) for the possible kinetic models computed by the linear and nonlinear regression methods. These values are compared with isoconversional  $E_{FR}$  values for the main decomposition step.  $E$  values correspond to the possible kinetic model and correlate with  $E_{FR}$  for neat polymers, which can be recognised

as additional evidence of the kinetic analysis accuracy. The non-isothermal decomposition of the mixtures, especially with catalysts added, is more complex in comparison with neat polymers. Regarding mixtures, calculated  $E$  values of possible kinetic models comply very well with the  $E_{FR}$  ones, and the difference between them is in the range of the experimental error. It can be concluded that suggested kinetic models can describe the non-isothermal decomposition of mixtures both with and without the presence of catalysts.

Figure 8 demonstrates above interpreted excellent correlation between experimental and calculated values. It proves that the suggested kinetic model fits the experimental data and provides a true description of the process complexity. Only the results for Mix 2/Fe are shown as an example since the comparison results of experimental data and the most suitable kinetic model calculated by linear or nonlinear regression model-fitting method showed good correlation.

**Fig. 8** Comparison of experimental data (points) and the most suitable kinetic model (solid lines) calculated by nonlinear regression model-fitting method for Mix 2/Fe



## Conclusion

The aim of this study was set to investigate the kinetics of the real-world plastic waste mixture pyrolysis and the effect of the prepared catalysts ( $\text{Fe}/\gamma\text{-Al}_2\text{O}_3$  and  $\text{Ni}/\gamma\text{-Al}_2\text{O}_3$ ) on its thermal decomposition mechanism. Kinetic analysis was performed so that later process could be scaled up for laboratory pyrolysis reactor. The mixture of real-world plastic waste (22% HDPE, 31% LDPE, 35% PP, 12% PS) was prepared according to the composition of post-consumer plastics waste in Europe (Mix 1). Second mixture (Mix 2) was prepared without PS (28% HDPE, 37% LDPE, 35% PP) to investigate the influence of PS on the reaction mechanisms of the thermal decomposition process. It was found that the non-isothermal decomposition of Mix 1 occurs in two decomposition steps while the non-isothermal decomposition of Mix 2 occurs in one decomposition step. It is concluded that the difference in the decomposition mechanism can be attributed to PS. The average value of activation energy calculated by isoconversional Friedman method for the thermal decomposition of Mix 1 was 205 kJ/mol and was decreased to 173 kJ/mol (15.6%) with the addition of  $\text{Fe}/\gamma\text{-Al}_2\text{O}_3$ , and 185 kJ/mol (9.8%) with  $\text{Ni}/\gamma\text{-Al}_2\text{O}_3$  catalyst. The value of average activation energy for Mix 2 was higher, 288 kJ/mol, and it decreased to 158 kJ/mol (45.1%) with the addition of  $\text{Fe}/\gamma\text{-Al}_2\text{O}_3$ , and 196 kJ/mol (31.9%) with  $\text{Ni}/\gamma\text{-Al}_2\text{O}_3$  catalyst. Mix 1 has lower average activation energy because PS starts decomposing at lower temperatures than HDPE, LDPE and PP. Finally, the application of  $\text{Fe}/\gamma\text{-Al}_2\text{O}_3$  and  $\text{Ni}/\gamma\text{-Al}_2\text{O}_3$  catalysts lowers the activation energy of all analysed samples, which confirms the set hypothesis. This indicates their potential for use in the pyrolysis process. In future, the experiments will be conducted with larger samples using  $\text{Fe}/\gamma\text{-Al}_2\text{O}_3$  catalyst as the kinetic study showed better results with this catalyst. The yield of the liquid and gaseous products without and with catalysts will be investigated.

**Acknowledgements** This work has been fully supported by the Croatian Science Foundation under the Project Neoplast (IP-2018-3200) and the project Career development of young researchers—the training of new Doctors of Science (DOK-2018-09-6944). This support is gratefully acknowledged.

## Appendix

Tables 5 and 6 present data containing the values of temperature maximum decomposition rate, maximum peak rate and final mass of the residue for the four heating rates of thermal decomposition of neat polymers (Table 5), and mixtures of polymers with and without catalyst used (Table 6). Bolded values in Table 6 show a significant change that occurred after the addition of catalysts to Mix

2 sample. Figure 9 shows thermogravimetric and derivative thermogravimetric plots of neat polymers at four heating rates. In Fig. 10 thermogravimetric and derivative thermogravimetric curves of neat polymers are compared at the heating rate of 10 °C/min.

**Table 5** The values of peak decomposition temperature, peak height and residue mass for the four heating rates (thermal decomposition of neat polymers) decomposition of neat polymers)

| Sample |                    | $\beta$ (°C/min) |       |       |       |
|--------|--------------------|------------------|-------|-------|-------|
|        |                    | 5                | 10    | 15    | 20    |
| HDPE   | $T_{\max}$ (°C)    | 463.7            | 476.6 | 484.0 | 491.3 |
|        | $r_{\max}$ (%/min) | 17.6             | 34.6  | 49.1  | 64.3  |
|        | $m_f$ (wt%)        | 2.8              | 3.3   | 2.9   | 2.7   |
| LDPE   | $T_{\max}$ (°C)    | 459.3            | 472.6 | 482.7 | 489.0 |
|        | $r_{\max}$ (%/min) | 17.6             | 33.2  | 45.6  | 63.2  |
|        | $m_f$ (wt%)        | 3.5              | 4.6   | 5.9   | 4.9   |
| PP     | $T_{\max}$ (°C)    | 441.0            | 457.7 | 466.6 | 474.1 |
|        | $r_{\max}$ (%/min) | 19.1             | 33.3  | 47.0  | 61.1  |
|        | $m_f$ (wt%)        | 0.9              | 2.3   | 1.4   | 0.8   |
| PS     | $T_{\max}$ (°C)    | 414.2            | 428.7 | 441.2 | 448.9 |
|        | $r_{\max}$ (%/min) | 11.9             | 23.5  | 29.6  | 37.1  |
|        | $m_f$ (wt%)        | 3.5              | 3.5   | 3.3   | 3.6   |

**Table 6** The values of peak decomposition temperature, peak height and residue mass for the four heating rates (thermal decomposition of polymer mixtures with and without with  $\text{Ni}/\gamma\text{-Al}_2\text{O}_3$  and  $\text{Fe}/\gamma\text{-Al}_2\text{O}_3$  catalysts)

| Sample   |                    | $\beta$ (°C/min) |              |              |              |
|----------|--------------------|------------------|--------------|--------------|--------------|
|          |                    | 5                | 10           | 15           | 20           |
| Mix 1    | $T_{\max}$ (°C)    | 471.3            | 489          | 498.2        | 507.3        |
|          | $r_{\max}$ (%/min) | 9.4              | 19           | 28.5         | 37           |
|          | $m_f$ (wt%)        | 2                | 1.5          | 2.5          | 3.5          |
| Mix 2    | $T_{\max}$ (°C)    | <b>457.7</b>     | <b>464.2</b> | <b>471.6</b> | <b>477.9</b> |
|          | $r_{\max}$ (%/min) | 14.2             | 30.8         | 46           | 61.3         |
|          | $m_f$ (wt%)        | 2                | 2.4          | 2.6          | 1.9          |
| Mix 1/Ni | $T_{\max}$ (°C)    | 471.6            | 489.7        | 496.5        | 509.3        |
|          | $r_{\max}$ (%/min) | 10.2             | 20.3         | 30.4         | 39.3         |
|          | $m_f$ (wt%)        | 4.8              | 3.7          | 4.7          | 5.3          |
| Mix 2/Ni | $T_{\max}$ (°C)    | <b>475.6</b>     | <b>496.4</b> | <b>507.8</b> | <b>513.6</b> |
|          | $r_{\max}$ (%/min) | 13.2             | 24.5         | 37.1         | 48           |
|          | $m_f$ (wt%)        | 3.3              | 4.2          | 3.9          | 4.3          |
| Mix 1/Fe | $T_{\max}$ (°C)    | 469.3            | 488.3        | 500          | 505.2        |
|          | $r_{\max}$ (%/min) | 9.7              | 19.4         | 29.3         | 37.6         |
|          | $m_f$ (wt%)        | 4.4              | 3.7          | 6.7          | 5.3          |
| Mix 2/Fe | $T_{\max}$ (°C)    | <b>475.6</b>     | <b>496.4</b> | <b>507.8</b> | <b>513.6</b> |
|          | $r_{\max}$ (%/min) | 13.2             | 24.5         | 37.1         | 48           |
|          | $m_f$ (wt%)        | 3.3              | 4.2          | 3.9          | 4.3          |

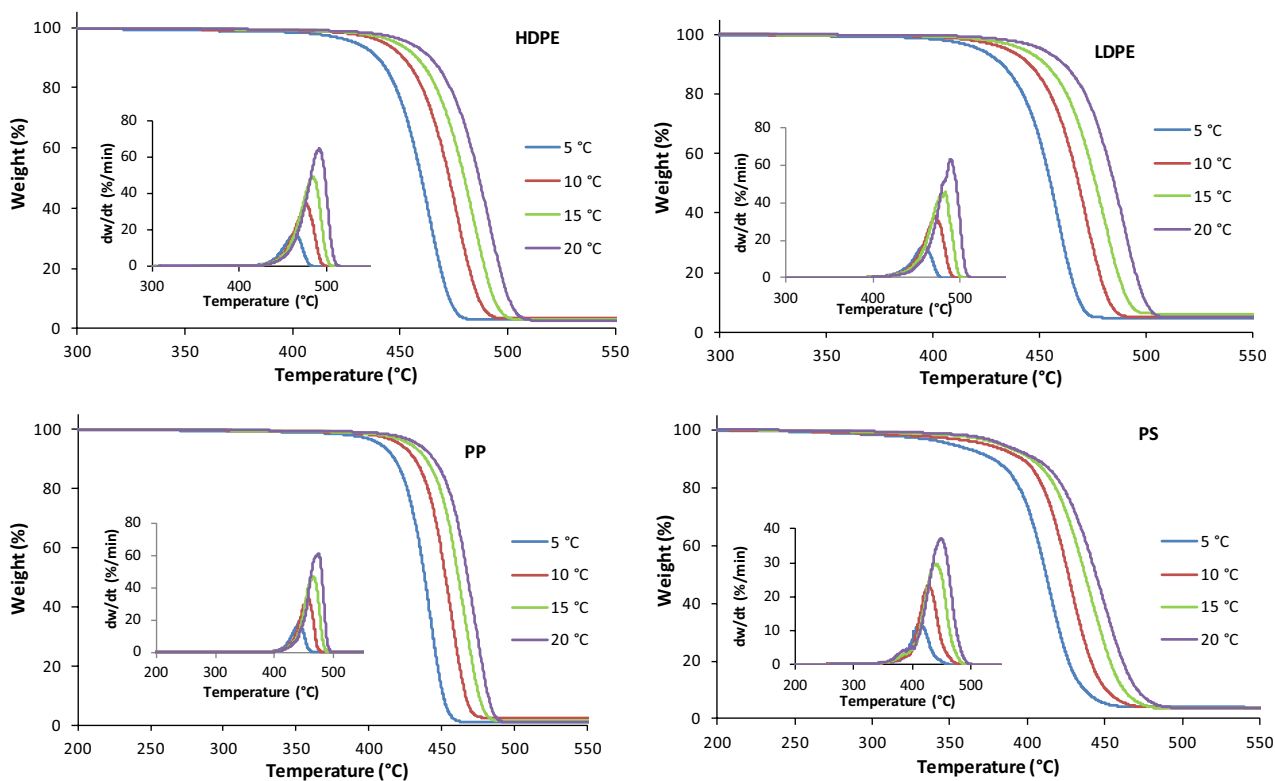


Fig. 9 Thermogravimetric and derivative thermogravimetric plots for HDPE, LDPE, PP and PS at 5, 10, 15 and 20 °C/min

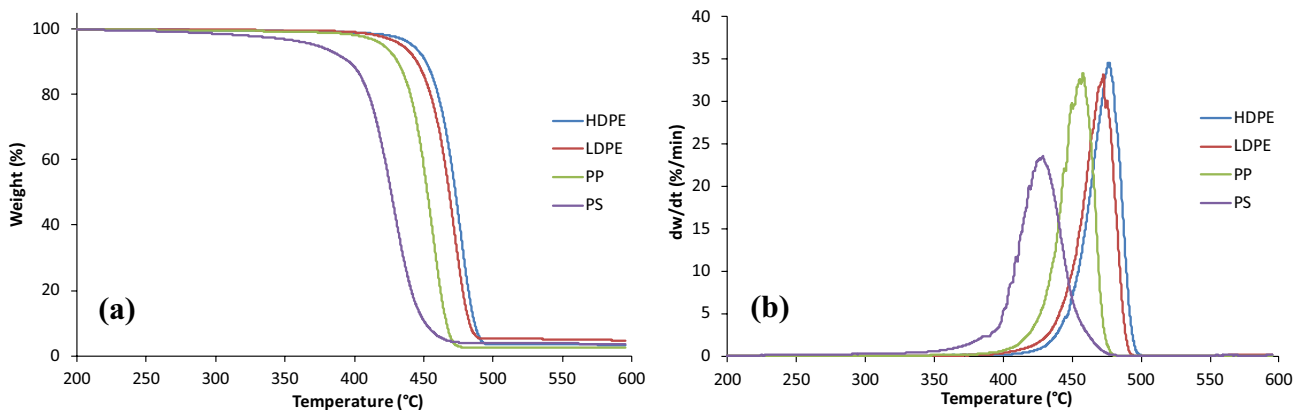


Fig. 10 a Thermogravimetric and b derivative thermogravimetric plot for HDPE, LDPE, PP and PS at 10 °C/min

## References

- Acomb JC, Wu C, Williams PT (2016) The use of different metal catalysts for the simultaneous production of carbon nanotubes and hydrogen from pyrolysis of plastic feedstocks. *Appl Catal B Environ*. <https://doi.org/10.1016/j.apcatb.2015.06.054>
- Al-Salem SM, Antelava A, Constantinou A et al (2017) A review on thermal and catalytic pyrolysis of plastic solid waste (PSW). *J Environ Manag* 197:177–198. <https://doi.org/10.1016/j.jenvman.2017.03.084>
- Antelava A, Damilos S, Hafeez S et al (2019) Plastic solid waste (PSW) in the context of life cycle assessment (LCA) and sustainable management. *Environ Manag* 64:230–244. <https://doi.org/10.1007/s00267-019-01178-3>
- Anuar Sharuddin SD, Abnisa F, Wan Daud WMA, Aroua MK (2016) A review on pyrolysis of plastic wastes. *Energy Convers Manag* 115:308–326. <https://doi.org/10.1016/j.enconman.2016.02.037>
- Benavides PT, Sun P, Han J et al (2017) Life-cycle analysis of fuels from post-use non-recycled plastics. *Fuel* 203:11–22. <https://doi.org/10.1016/j.fuel.2017.04.070>
- Das P, Tiwari P (2017) Thermal degradation kinetics of plastics and model selection. *Thermochim Acta* 654:191–202. <https://doi.org/10.1016/j.tca.2017.06.001>
- Diaz Silvarrey LS, Phan AN (2016) Kinetic study of municipal plastic waste. *Int J Hydrog Energy*. <https://doi.org/10.1016/j.ijhydene.2016.05.202>
- El Hanandeh A (2013) Carbon abatement via treating the solid waste from the Australian olive industry in mobile pyrolysis units: LCA with uncertainty analysis. *Waste Manag Res* 31:341–352. <https://doi.org/10.1177/0734242X12465317>
- Erceg M, Krešić I, Vrandečić NS, Jakić M (2018) Different approaches to the kinetic analysis of thermal degradation of poly(ethylene oxide). *J Therm Anal Calorim* 131:325–334. <https://doi.org/10.1007/s10973-017-6349-6>
- Friedman H (1964) Kinetics of thermal degradation of char-forming plastics from thermogravimetry. Application to a phenolic plastic. *J Polym Sci*. <https://doi.org/10.1002/polc.5070060121>
- Ghorbannezhad P, Park S, Onwudili JA (2020) Co-pyrolysis of biomass and plastic waste over zeolite- and sodium-based catalysts for enhanced yields of hydrocarbon products. *Waste Manag* 102:909–918. <https://doi.org/10.1016/j.wasman.2019.12.006>
- Imani Moqadam S, Mirdrikvand M, Roozbehani B et al (2015) Polystyrene pyrolysis using silica-alumina catalyst in fluidized bed reactor. *Clean Technol Environ Policy* 17:1847–1860. <https://doi.org/10.1007/s10098-015-0899-8>
- Khoo HH (2019) LCA of plastic waste recovery into recycled materials, energy and fuels in Singapore. *Resour Conserv Recycl* 145:67–77. <https://doi.org/10.1016/j.resconrec.2019.02.010>
- Miandad R, Barakat MA, Aburiazza AS et al (2016) Catalytic pyrolysis of plastic waste: a review. *Process Saf Environ Prot* 102:822–838. <https://doi.org/10.1016/j.psep.2016.06.022>
- Miskolczi N, Sója J, Tulok E (2017) Thermo-catalytic two-step pyrolysis of real waste plastics from end of life vehicle. *J Anal Appl Pyrol*. <https://doi.org/10.1016/j.jaap.2017.11.008>
- Netzsch Gerätebau GmbH (2014) Netzsch thermokinetics software manual. Netzsch Gerätebau GmbH, Selb
- Opfermann J (2000) Kinetic analysis using multivariate non-linear regression. I. Basic concepts. *J Therm Anal Calorim* 60:641–658. <https://doi.org/10.1023/A:1010167626551>
- Peterson JD, Vyazovkin S, Wight CA (2001) Kinetics of the thermal and thermo-oxidative degradation of polystyrene, polyethylene and poly(propylene). *Macromol Chem Phys*. [https://doi.org/10.1002/1521-3935\(20010301\)202:6%3c775:AID-MACP775%3e3.0.CO;2-G](https://doi.org/10.1002/1521-3935(20010301)202:6%3c775:AID-MACP775%3e3.0.CO;2-G)
- Plastics – the Facts (2019) An analysis of European latest plastics production, demand and waste data. Plastics Europe. <https://www.plasticseurope.org/en/>. Accessed 11 Dec 2019
- Ragaert K, Delva L, Van Geem K (2017) Mechanical and chemical recycling of solid plastic waste. *Waste Manag* 69:24–58. <https://doi.org/10.1016/j.wasman.2017.07.044>
- Riad M (2007) Influence of magnesium and chromium oxides on the physicochemical properties of  $\gamma$ -alumina. *Appl Catal A* 327:13–21. <https://doi.org/10.1016/j.apcata.2007.04.027>
- Roozbehani B, Motevassel M, Mirdrikvand M et al (2017) Gasoline production from a polymeric urban disposal mixture using silica-alumina catalyst. *Clean Technol Environ Policy* 19:123–136. <https://doi.org/10.1007/s10098-016-1196-x>
- Rotaru A, Goşa M (2009) Computational thermal and kinetic analysis: complete standard procedure to evaluate the kinetic triplet form non-isothermal data. *J Therm Anal Calorim* 97:421–426. <https://doi.org/10.1007/s10973-008-9772-x>
- Rotaru A, Goşa M, Rotaru P (2008) Computational thermal and kinetic analysis: software for non-isothermal kinetics by standard procedure. *J Therm Anal Calorim* 94:367–371. <https://doi.org/10.1007/s10973-008-9108-x>
- Sakaki SA, Roozbehani B, Shishesaz M, Abdollahkhani N (2014) Catalytic degradation of the mixed polyethylene and polypropylene into middle distillate products. *Clean Technol Environ Policy* 16:901–910. <https://doi.org/10.1007/s10098-013-0688-1>
- Sánchez-Jiménez PE, Pérez-Maqueda LA, Perejón A, Criado JM (2013) Clarifications regarding the use of model-fitting methods of kinetic analysis for determining the activation energy from a single non-isothermal curve. *Chem Cent J*. <https://doi.org/10.1186/1752-153X-7-25>
- Singh RK, Ruj B, Sadhukhan AK, Gupta P (2019a) A TG-FTIR investigation on the co-pyrolysis of the waste HDPE, PP, PS and PET under high heating conditions. *J Energy Inst*. <https://doi.org/10.1016/j.joei.2019.09.003>
- Singh RK, Ruj B, Sadhukhan AK, Gupta P (2019b) Impact of fast and slow pyrolysis on the degradation of mixed plastic waste: product yield analysis and their characterization. *J Energy Inst* 92(6):1647–1657. <https://doi.org/10.1016/j.joei.2019.01.009>
- Straka P, Bičáková O, Šupová M (2017) Thermal conversion of polyolefins/polystyrene ternary mixtures: kinetics and pyrolysis on a laboratory and commercial scales. *J Anal Appl Pyrol* 128:196–207. <https://doi.org/10.1016/j.jaap.2017.10.010>
- Tomić T, Schneider DR (2018) The role of energy from waste in circular economy and closing the loop concept: energy analysis approach. *Renew Sustain Energy Rev* 98:268–287. <https://doi.org/10.1016/j.rser.2018.09.029>
- Vrandečić NS, Erceg M, Jakić M, Klarić I (2010) Kinetic analysis of thermal degradation of poly(ethylene glycol) and poly(ethylene oxide)s of different molecular weight. *Thermochim Acta* 498:71–80. <https://doi.org/10.1016/j.tca.2009.10.005>
- Vyazovkin SV, Lesnikovich AI (1990) An approach to the solution of the inverse kinetic problem in the case of complex processes. Part I. Methods employing a series of thermoanalytical curves. *Thermochim Acta*. [https://doi.org/10.1016/0040-6031\(90\)80227-P](https://doi.org/10.1016/0040-6031(90)80227-P)
- Vyazovkin S, Sbirrazzuoli N (2006) Isoconversional kinetic analysis of thermally stimulated processes in polymers. *Macromol Rapid Commun* 27:1515–1532. <https://doi.org/10.1002/marc.200600404>
- Vyazovkin S, Burnham AK, Criado JM et al (2011) ICTAC Kinetics Committee recommendations for performing kinetic computations on thermal analysis data. *Thermochim Acta* 520:1–19. <https://doi.org/10.1016/j.tca.2011.03.034>
- Wang J, Jiang J, Meng X et al (2020) Promoting Aromatic Hydrocarbon Formation Via Catalytic Pyrolysis Of Polycarbonate Wastes

- over Fe- and Ce-loaded aluminum oxide catalysts. *Environ Sci Technol* 54:8390–8400. <https://doi.org/10.1021/acs.est.0c00899>
- Yao D, Zhang Y, Williams PT et al (2018) Co-production of hydrogen and carbon nanotubes from real-world waste plastics: Influence of catalyst composition and operational parameters. *Appl Catal B Environ*. <https://doi.org/10.1016/j.apcatb.2017.09.035>
- Zaman AU (2010) Comparative study of municipal solid waste treatment technologies using life cycle assessment method. *Int J Environ Sci Technol* 7:225–234. <https://doi.org/10.1007/BF03326132>
- Zhang H, Nie J, Xiao R et al (2014) Catalytic co-pyrolysis of biomass and different plastics (polyethylene, polypropylene, and polystyrene) to improve hydrocarbon yield in a fluidized-bed reactor. *Energy Fuels*. <https://doi.org/10.1021/ef4019299>

**Publisher's Note** Springer Nature remains neutral with regard to jurisdictional claims in published maps and institutional affiliations.

## Affiliations

Irma Kremer<sup>1</sup> · Tihomir Tomić<sup>1</sup> · Zvonimir Katančić<sup>2</sup> · Zlata Hrnjak-Murgić<sup>2</sup> · Matko Erceg<sup>3</sup> · Daniel R. Schneider<sup>1</sup>

<sup>1</sup> Department of Energy, Power Engineering and Environment, Faculty of Mechanical Engineering and Naval Architecture, University of Zagreb, Zagreb, Croatia

<sup>2</sup> Department of Polymer Engineering and Organic Chemical Technology, Faculty of Chemical Engineering and Technology, University of Zagreb, Zagreb, Croatia

<sup>3</sup> Department of Organic Technology, Faculty of Chemistry and Technology, University of Split, Split, Croatia